

Novel total hip surgery robotic system based on self-localization and optical measurement

Weibo Ning^a, Jiaqi Zhu^a, Hongjiang Chen^b, Weijun Zhou^a, Shuxing He^a, Yecheng Tan^a, Qianrui Xu^a, Ye Yuan^a, Jun Hu^b and Zhun Fan^a

^aShantou University, Shantou, China

^bThe First Affiliated Hospital of Medical College of Shantou University, Shantou, China

ARTICLE INFO

Keywords:

Total hip arthroplasty
Surgery navigation
End-effector
Optical positioning
Femoral neck length

ABSTRACT

This paper presents the development and experimental evaluation of a surgical robotic system for total hip arthroplasty (THA). Although existing robotic systems used in joint replacement surgery have achieved some progresses, the robot arm must be situated accurately at the target position during operation, which depends significantly on the experience of the surgeon. In addition, handheld acetabulum reamers typically exhibit uneven strength and grinding file. Moreover, the lack of techniques to real-time measure femoral neck length may lead to poor outcomes. To tackle these challenges, we propose a real-time traceable optical positioning strategy to reduce unnecessary manual adjustments to the robotic arm during surgery, an end-effector system to stabilise grinding, and an optical probe to provide real-time measurement of the femoral neck length and other parameters used to choose the proper prosthesis. The lengths of the lower limbs are measured as the prosthesis is installed. The experimental evaluation results show that, based on its accuracy, execution ability, and robustness, the proposed surgical robotic system is feasible for THA.

1. Introduction

Total hip arthroplasty (THA) is one of the most important methods used to alleviate the symptoms of patients with hip diseases [1–3]. Unfortunately, the quality of traditional THA surgery relies heavily on the experience of surgeons. Because its intraoperative field of vision is limited, it can easily lead to incorrect size choices and placement of prostheses. There may also be other complications, such as early dislocation and postoperative leg length discrepancy, among others [4–6]. To address these problems, Lewinnek et al. [7] suggested reducing postoperative complications by focusing upon the normal angle range of acetabular prosthesis placement, i.e. the abduction angle is $40^\circ \pm 10^\circ$, whereas the anteversion angle is $15^\circ \pm 10^\circ$. During the operation, it is difficult for a surgeon to correctly place the prosthesis because of the lack of positioning information [8, 9]. Thus, Widmer et al. [10] used a trigonometric function relationship to determine the positioning of an acetabular cup using X-ray imaging. However, the disadvantage is radiation exposure and additional skin incisions, which increases other accidental risks. On the other hand, Dechenne et al. [11] used a mechanical equipment to select anatomical bone markers to correctly place an acetabular prosthesis. However, the device is based on an ideal surgical scheme and hard to generalize.

Postoperative leg length discrepancy remains the most common cause of patient dissatisfaction and malpractice litigation in hip arthroplasty [12–14]. It is important to choose appropriate lengths for femoral head prostheses and to minimise inequalities between both lower limbs after

the operation, enabling patients to recover faster. Several methods have been proposed for adjusting the length of the femoral neck during surgery. For example, Kyoichio et al. [15] used a measuring device similar to a Vernier caliper. Tagomori et al. [16] used a ruler to measure the marked position of the posterior acetabulum prior to dislocation. However, the disadvantage of these mechanical structures is that the deployment of measuring equipment requires direct intervention on the surgical lesion of the patient, which may interfere with the operation performed by the surgeon. In addition, these devices are not convenient for surgeons to read.

Recently, the clinical efficacy of surgical robots has become a hot topic joint surgery [17]. It has been reported that robot-assisted THA can improve the precision of prosthesis placement and have advantages over conventional THA in reducing the difference between the lower limbs [18–20]. A wider implementation of robotic surgery is thus expected as surgeons become more familiar with this technology [21, 22]. The clinical outcome may be improved through the selection of an appropriate grinding angle and femoral neck length, thus reducing inequality in the lengths of the lower limbs after the operation. Currently, commercial hip surgery robots use visual navigation technologies to guide surgeons to accurately and quickly place prostheses with the help of external tracking devices [23, 24]. In early 2007, RoboDoc (Integrated Surgical Systems, USA) obtained results comparable to those of traditional surgical procedures [25]. Hip surgery robots currently available in the market, such as MAKO (Stryker, USA), have also achieved satisfactory results in assisting THA. Their navigation systems ensure accurate placement of acetabular prostheses [26, 27]. However, they still have the following three shortcomings: First, the cost is high, and thus the

*Corresponding author

**Corresponding author

***Corresponding author:
ORCID(s):

popularity is low. Second, during the operation, surgeons must drag the robot arm into position, which requires good clinical experience. Third, because the length of the femoral neck and the difference between both lower limbs cannot be measured during the operation, the manipulation process is highly dependent on the registration process for image space and surgical space. As a result, the operation accuracy also depends on the registration accuracy. Moreover, the real-time registration process is complicated, and the learning curve for the surgical procedure is long [28, 29].

Therefore, in this paper, based on the principle of optical localisation, a method based on real-time tracking and positioning is proposed to facilitate accurately measuring distances and operating robotic arms during surgery, which can not only improve the efficiency of prosthesis positioning, but also significantly reduce the chance of inequality in the lengths of the lower limbs after the operation. In summary, an imageless surgical navigation system based on optical positioning is proposed in this work, in which the femoral neck length is measured in real time using a probe, so that postoperative complications can be largely reduced via comparisons between the lengths of the lower limbs during the surgery. In addition, an end-effector system is developed to enable stable grinding and improve surgical safety.

2. FRAMEWORK DESIGN

2.1. Total Hip Arthroplasty Robot System

In this study, we developed a surgical robot based on optical positioning and a multi-degree-of-freedom flexible robotic arm to help surgeons eliminate subjective errors and improve the quality of hip-replacement surgery. The framework of the robotic system consists of preoperative planning and intraoperative execution (Figure 1). After preoperative 3D CT reconstruction, grinding path planning and hand-eye calibration were performed. The calibration and navigation systems were designed based on an optical positioning system to be used during the operation. It is very important to obtain accurate target position information from the calibrator and intraoperative navigation system to reduce errors during surgery. To facilitate the surgery operations, an end-effector system to be applied on the 6-DOF flexible robotic arm was also designed and developed, which had robust signal acquisition and feedback functions. Further details are provided in sections II-B, II-C, and II-D.

2.2. Calibrators and Image Processing

The calibration tool developed in this study is fixed onto the end of the robotic arm through a flange (Figure 2). A new coordinate system was obtained through corresponding adjustments on the offset of the centre of the end flange. Therefore, the dimension parameters from the end flange connection centre to the marker ball centre would be calculated using the design drawing of the calibrator. The coordinate information of the marker ball centre was read from the base coordinates of the manipulator. The movement of the robotic arm was controlled with a preset

step length, and the sequence of position information of the centre of the marker ball installed in the optical positioning instrument with reference to the robotic arm base coordinate system was then recorded. Based on singular value decomposition, as demonstrated in literature [30, 31], a novel algorithm with added error filtering (as illustrated in Algorithm 1) was used to calculate the hand-eye conversion relationship H_{base}^{cam} . In accordance with the transformation relationship of the coordinates $H_{base}^{pic} = H_{cam}^{pic} \cdot H_{base}^{cam}$, the transform matrix H_{base}^{pic} was calculated to complete the path positioning. Furthermore, after the surgeon planned a proper grinding path on the image, the robot could move accurately according to it. Particularly, H_{base}^{pic} is the transformation from the image space to the base coordinate system of the robot arm. H_{cam}^{pic} is the transformation from the image space to the coordinate system of the optical locator. H_{base}^{cam} is the transformation from the optical locator to the base coordinate system of the robot arm.

Algorithm 1 Robotic calibration process for total hip surgery

Require: Plan the initial point and step size of the robotic arm movement

- 1: The robot arm moves according to the corresponding step length and records the hand-eye point pair set P, Q
 - 2: P and Q are averaged: \bar{P}, \bar{Q}
 - 3: Subtract the mean (center point) from the data: $\tilde{P} = P - \bar{P}, \tilde{Q} = Q - \bar{Q}$
 - 4: Matrix calculation: $H = \tilde{P}^T \cdot \tilde{Q}$
 - 5: SVD decomposition: $U, S, V = SVD(H)$
 - 6: Rotation matrix calculation: $R = V \cdot U^T$
 - 7: Reflection matrix detection
 - 8: Translation matrix calculation: $T = -R \cdot \bar{P}^T + \bar{Q}^T$
 - 9: Invert the robotic arm's coordinate point set using a P point set: $P_1 = R \cdot P + T$
 - 10: Error calculation: $\alpha = P - P_1$
 - 11: **if** $\alpha = P - P_1 < \beta$ **then**
 - 12: **return** R, T
 - 13: **else**
 - 14: **repeat**
 - 15: Reject the set of points with significant errors, and repeat steps 3 through 11
 - 16: **until** $\alpha = P - P_1 < \beta$
 - 17: **end if**
 - 18: **return** R, T
-

After the hand-eye calibration, a 3D reconstruction of CT images of the hip bones was performed (as shown in Figure 3). In the reconstructed 3D model, the abduction angle, forward inclination angle, and cartilage thickness of the acetabular grinding were determined to plan the grinding path of the end actuator of the robotic arm. The 3D reconstruction model was then converted into a 3D point cloud, with the vertices of each marker ball selected, and the contours of each marker ball in the image coordinate system segmented using the Kd-Tree algorithm. Through the least

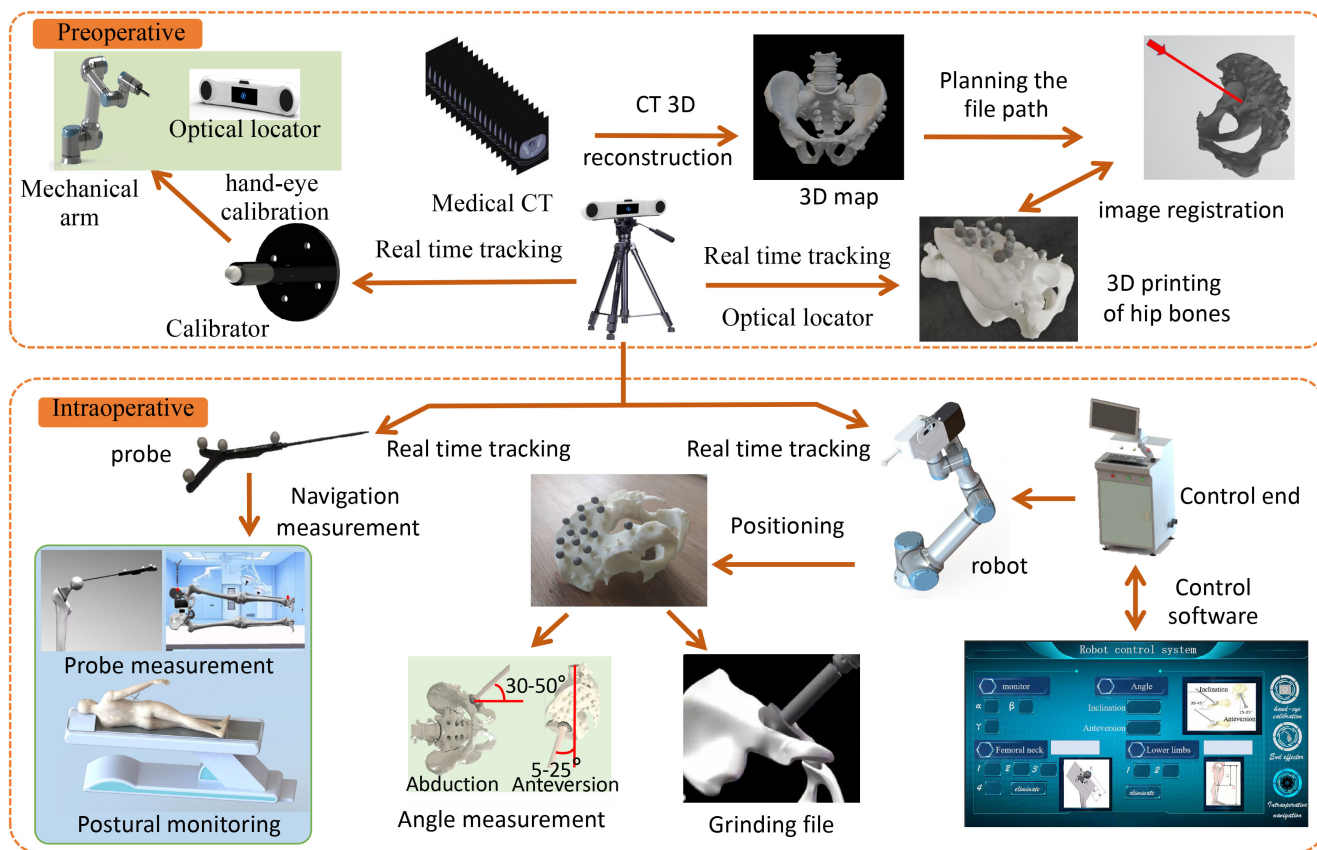


Figure 1: Frame of autonomous-navigation THA robot system.

squares method, the contour of each marker ball in the image coordinate system was fitted, and its centre coordinates were obtained. At the same time, the actual hip model was placed in the field of view of the optical locator, and then the spherical coordinates of the marker balls were collected. The transformation relationship between the optical locator and the image coordinate system was then calculated using the principle of Algorithm 1 to complete the matching between the image and the actual hip model.

2.3. End Actuators

The end-effector of the surgical robot is used in the process of acetabular grinding. Its structural composition is shown in Figure 4. As shown in Figure 5, the user could obtain the movement information of the end-effector and contact pressure using the remote host computer and send control instructions to the microcontroller system through the wireless module. The microcontroller system sent control signals to both the stepper motor and the acetabulum reamer motor. During this process, we used optical positioning systems to track the marker balls, visualized their movements in real time, and passed them to the host computer controller. Simultaneously, a pressure sensor was used to obtain the contact pressure of the reamer as feedback. A database was then established to store the parameters corresponding to the reamer pressure and filing

amount in a clinical experiment. If the pressure reached a threshold, the end-effector could be stopped in time to avoid excessive pressure during the grinding process, which would otherwise harm the patient. In future studies, with more sufficient data collected and more advanced control algorithms developed, the acetabulum reamer will grind more safely.

2.4. Intraoperative Measurement and Navigation

This study proposes a control scheme for the spatial measurement of key points in hip replacement surgery. The hip model was placed in the lateral recumbent position. In the self-designed position monitoring calibration tool, the established human body coordinate system of the patient was used as the reference coordinate system, enabling real-time changes in the intraoperative patient position to be monitored using the display of the surgical navigation interface. A rigid body coordinate system was established using three noncollinear marker balls at the end of the device. The end-effector was parallel to the desktop and placed according to the optical positioning system. The spatial coordinate information was initialised to zero. When the reamer on the end-effector was positioned, the rigid body coordinate system was visualised in real-time relative to the spatial information. This could assist surgeons to determine whether the grinding angle is within the normal range. To improve the accuracy of

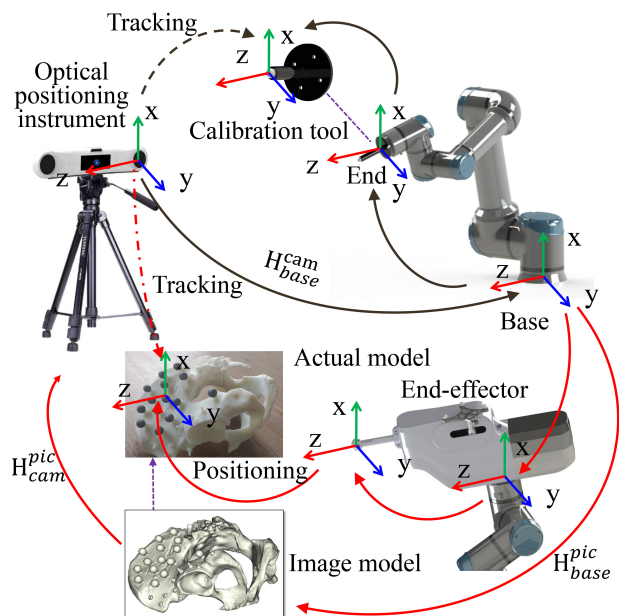


Figure 2: Robot arm - Optical locator - Calibration tool - Calibration of end-effector. Setup for coordinate system transformation of robot for target positioning.

the grinding angle measurement, we proposed a method for adjusting the robotic arm attitude based on real-time optical feedback. After the transformation relationship between the optical locator and the base coordinate system of the robotic arm is obtained according to Algorithm 1, the desired value of the angle of the robotic arm could be calculated via the input of the desired value into the optical locator coordinate system. The error between the desired and true values, as obtained using the optical locator, could be added to the desired value. Thus, the angle of the robot arm was adjusted based on the error as the input value. This procedure was iterated continuously until the error satisfies the requirements.

Subsequently, an intraoperative image-free measurement scheme based on optical positioning probes was proposed. After the length of the femoral neck was measured using a probe during the operation, an appropriate femoral ball prosthesis model could be selected in real-time to effectively reduce the postoperative leg length discrepancy. Then it was further verified according to the difference in the length of both lower limbs.

3. METHODOLOGY

The research protocol for the complete surgical procedure was as follows: Preoperative - A hip model with optical spheres (Figure 6b, male, PVC material) was prepared, and it was a 3D reconstruction based on a preoperative CT scan created to determine the planned surgical path. Intraoperative - A position monitoring tool was first installed to complete the calibration process. Clamps were used to secure the hip bone to the operating table in the lateral recumbent position (Figure 6a), and the robot completed

the calibration positioning. The intraoperative precision navigation system measured the grinding angle in real-time (e.g. abduction angle $40^\circ \pm 10^\circ$, forward inclination angle $15^\circ \pm 10^\circ$), thus verifying the control function of the end-effector during the grinding process. For this study, we used the intraoperative navigation system on a 1:1 skeletal model of the human body (Figure 6e, male, PVC material). Protocol: The optical probe (Figure 6d) was used to measure the length of the femoral neck, lengths of both lower limbs, as well as other parameters. The caliper and combined angle ruler were used to measure the length of the femoral neck for comparison. The ankle was fixed above the calibration pad. A piece of millimetre paper was placed under the pad (Figure 6f), and a fixed reference block was positioned in the hip (Figure 6g). Several different experimental situations were provided, e.g. the two lower limbs move at different distances from the pad, to test the accuracy of the measurement scheme.

3.1. Test 1

The purpose of the first test was to evaluate the accuracy of the positioning of the robot. As shown in Figure 2, we used a self-developed calibration tool to verify the transformation accuracy of the entire machine based on the optical locator, robotic arm, and image space coordinate system.

1) The operator selected the initial posture A_0 of the calibration tool at the end of the robotic arm before surgery [32], which was in the field of view of the optical locator. Once the initial posture was determined, the calibration tool was moved by a certain step length in subsequent calibration steps.

2) Based on the error between the inversed and actual robot arm coordinates, the threshold value was set to 2 mm. The system then calculated the optimal rotation matrix R and translation matrix T between the point sets in the coordinate system of the manipulator and the optical positioner.

3.2. Test 2

The purpose of this study was to evaluate the functionality of the grinding angle measurement of the end-effector in real-time during the surgery.

1) The hip was fixed onto the experimental platform, and the grinding and filing angles were measured in real-time during the simulated operation.

2) After the surgeon planned the grinding angle in the image space, the angle was converted to the coordinate system of the robotic arm by the optical locator. The robot autonomously reached the target position accordingly, and the optical locator read the spatial position of the optical sphere at the end of the device in real-time, thereby obtaining the angle error value. The desired value of the optical locator, pulsing the error value, was used as the input, with the angle error threshold value set to 0.5° . Iteration continued until the experimental requirements were satisfied.

3.3. Test 3

This test was performed to verify the control functionality of the end-effector. After the arm was positioned in

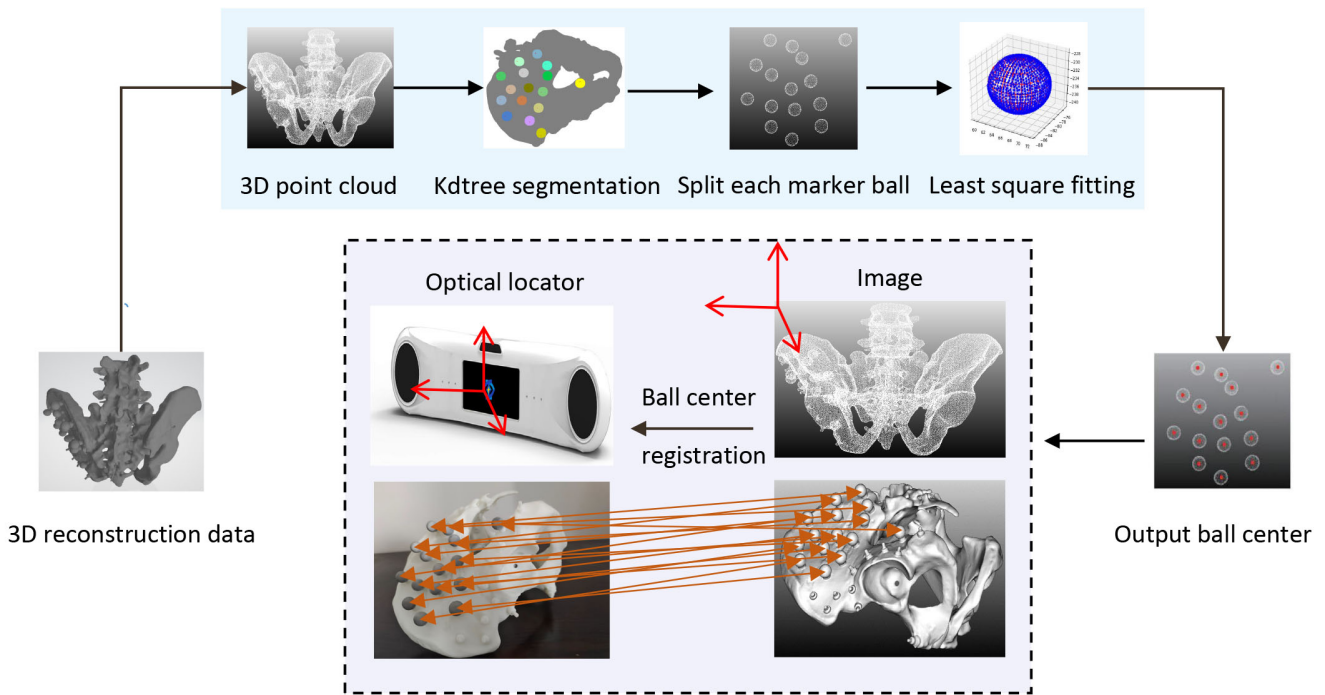


Figure 3: Surgical registration based on image registration.

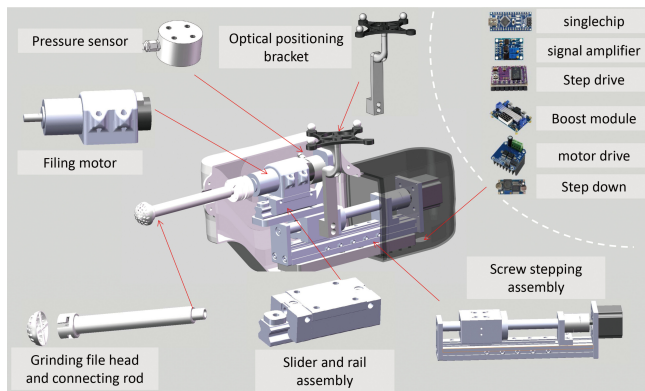


Figure 4: Structure composition diagram of the end-effector.

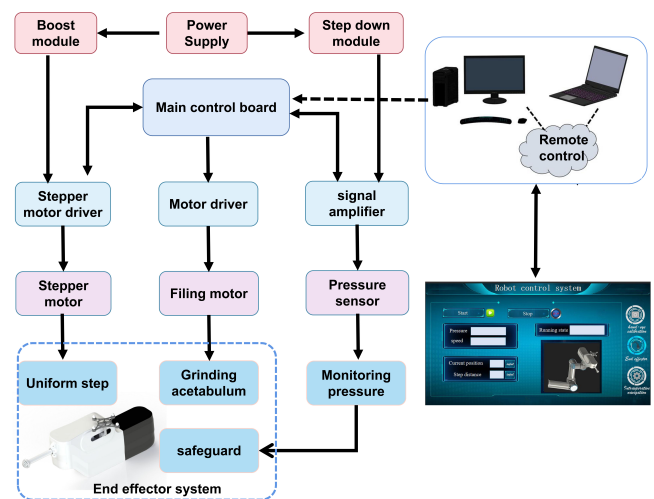


Figure 5: Principle of end-effector.

the right place, it was locked. The reamer was then moved by the stepper motor. When it contacted the acetabular, the grinding motor automatically starts. Driven by the stepper motor, it grounded the hip bone evenly in a fixed direction. Simultaneously, real-time pressure detection was performed, with the safety threshold set to 30 N. When the pressure reached the threshold value, the grinding process stopped and the system was reset.

3.4. Test 4

This test was performed to evaluate the intraoperative measurement of femoral neck length and differences in lower limbs. The experimental setup is shown in Figure 7. First, femoral neck length was measured using an optical posi-

tioning probe. The measurements were repeated 10 times. Second, a scenario was given simulating the measurement of the difference between the two legs after surgery, in which the left and right legs were moved along the longitudinal direction of the millimetre paper by 5 mm and 10 mm, alternately. This step was repeated 10 times.

1) As shown in Figure 7a, a 3D printed model (composed of a femur stalk inserted into a femur) was used to simulate anatomy measurement during surgery. The actual length c of the rotation centre of the femoral head to the femoral

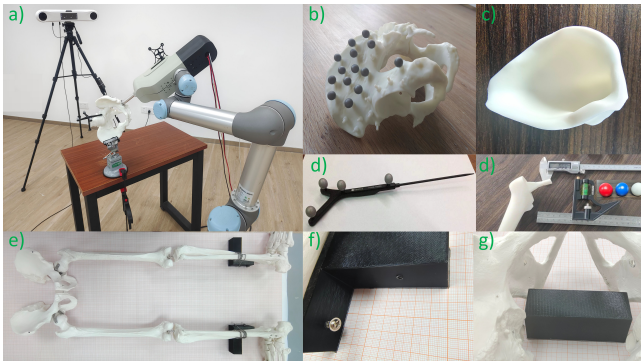


Figure 6: Simulation of experimental protocol for positioning and calibration system during surgery.

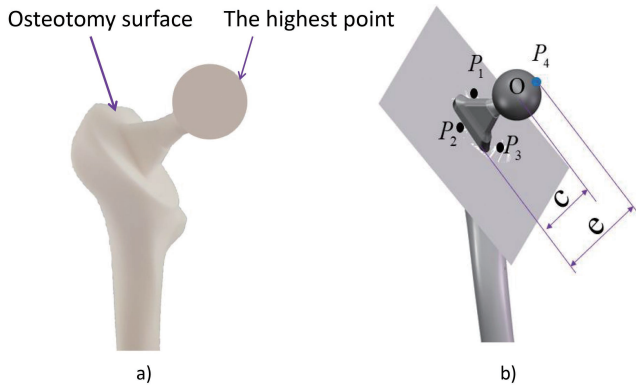


Figure 7: Intraoperative measurement of femoral neck length.

surface was obtained using the end of an optical probe, which measured the distance from the highest point to the osteotomy surface, subtracted the radius of the femoral head prosthesis (Figure 7b). The coordinates $P_1 (x_1, y_1, z_1)$, $P_2 (x_2, y_2, z_2)$, and $P_3 (x_3, y_3, z_3)$ of the three reference points were obtained sequentially from the osteotomy surface of the affected limb, and the coefficients A , B , C , and D of the osteologic surface equation were calculated using equation (1).

$$Ax + By + Cz + D = 0 \quad (1)$$

The measurement point of the femoral spheroid prosthesis was the highest point, $P_4 (x_4, y_4, z_4)$, on the femoral spherical prosthesis. The formula (2) was used to calculate the distance between the osteotomy surface of the affected limb and the measurement point e .

$$e = \frac{Ax + By + Cz + D}{\sqrt{A^2 + B^2 + C^2}} \quad (2)$$

where x , y , and z represented the coordinate values of the measurement points; and e represented the distance between the osteotomy surface of the affected limb and the measurement point.

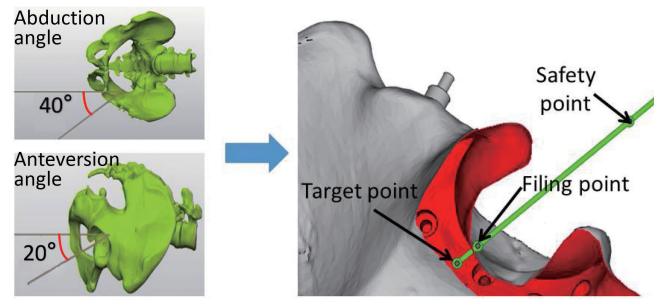


Figure 8: Preoperative robot reamer entry path planning.

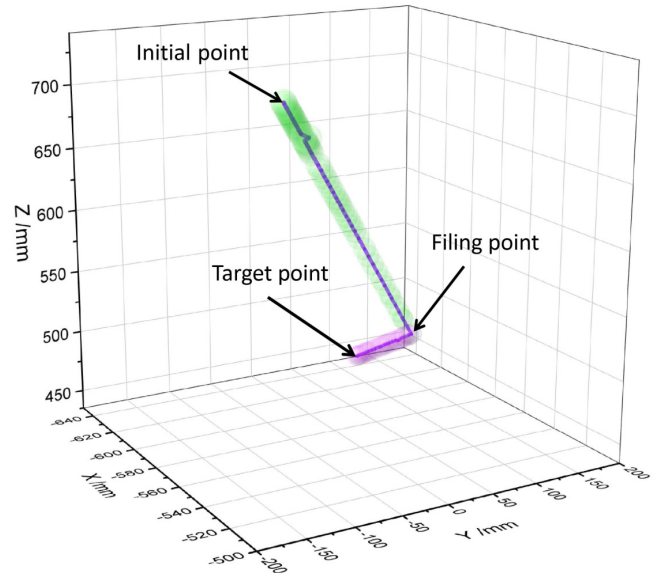


Figure 9: Trajectory of robotic arm.

2) The simulation compensated for errors in the operation by selecting different types of femoral head prostheses.

3) After the prosthesis was installed, the length of the affected leg was measured in real time. We compared the values with those obtained from preoperative measurements.

4. RESULTS & DISCUSSION

4.1. Calibration of Positioning Control by Surgical Robot

Preoperative surgical path planning (Figure 8) was performed to determine the optimal grinding angle of the robot, with the safe point, grinding point, and target point being shown in the image space.

The actual motion trajectory of the reamer at the end of the manipulator during surgery (Figure 9) required the calculation of the spatial distance between its desired and measured positioning values. As shown in Figure 10, the average Euclidean errors generated in the experiment, included 0.72 mm in the x-axis direction, 0.71 mm in the y-axis direction, and 0.69 mm in the z-axis direction, was 1.51 mm.

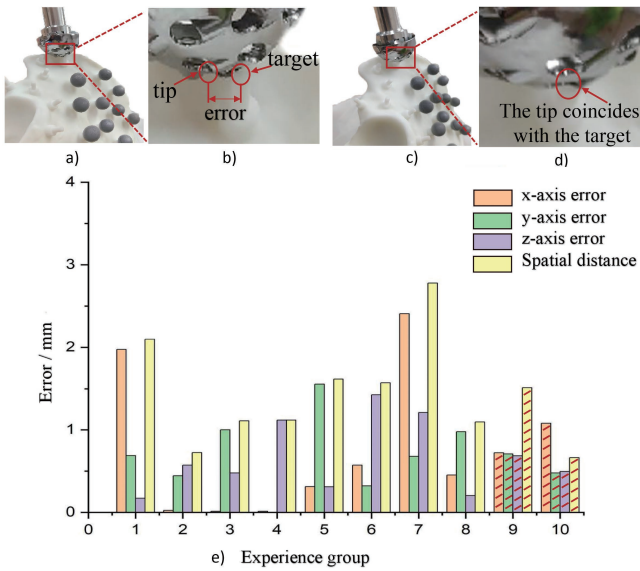


Figure 10: Surgical robot calibration experiment. a) Expected value of robot arm positioning. b) local enlarged view of a). c) real value of robot arm positioning. d) local enlarged view of c). e) histogram of positioning accuracy of grinding file tip. Zones 1 through 8 represent Euclidean distance directional error, and zones 9 and zone 10 represent mean error and standard deviation (SD).

4.2. Evaluation of Robot Measurement Navigation System

The measurement results of the surgical robot for the hip morphological parameters of the patient were as follows: When the robot reached the desired coordinate point, if no feedback adjustment was added, the average errors of the forward tilt angle and abduction angle (Figure 11a, Figure 11c) were 0.99° and 1.79° , respectively. After feedback was added to adjust the attitude of the robot, the average errors of the forward tilt angle and abduction angle (Figure 11b, Figure 11d) were 0.22° and 0.15° , respectively. After the robot arm reached the desired value, the output data of the optical positioner was fed back to improve the accuracy of the grinding angle. According to CAD models of the femoral neck prostheses, the sizes of the red, blue, and white femoral heads were 58, 59, and 60 mm, respectively. As shown in Figure 12, the average error of the distance from the highest point of femoral bulb prosthesis to the osteotomy surface, as measured using optical probes, were 0.071, 0.118, and 0.087 mm, respectively. For comparison, the average errors measured using the mechanical equipment were 0.287, 0.278, and 0.307 mm. Thus, it was demonstrated that the optical probe had much higher precision and could effectively assist surgeons in performing THA surgery.

Based on data in Table 1, the following conclusions could be drawn. When the two lower limbs did not move, the average difference between the two lower limbs was 0.17 mm. When the affected limb moved down 5 mm and 10 mm longitudinally, the average differences between the

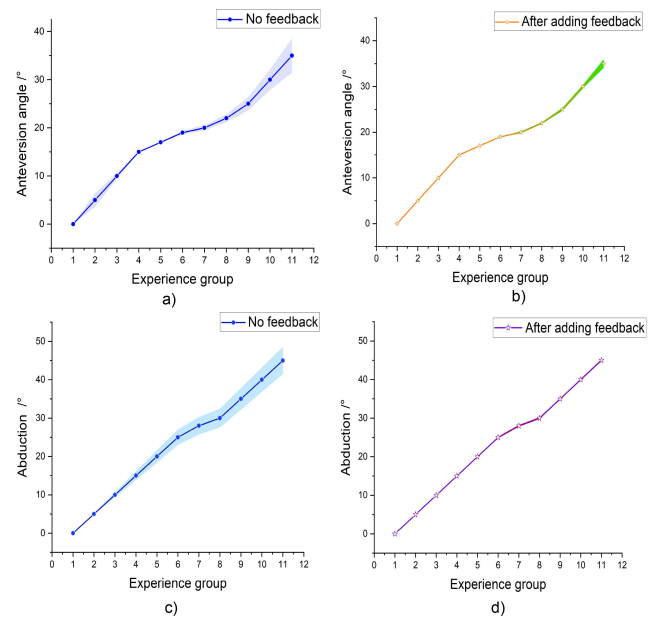


Figure 11: Real-time measurement of grinding angle after positioning of the robotic arm. a) and c) are error band diagrams of the anteversion and abduction angles without feedback. b) and d) are the error band diagram of the anteversion and abduction angles after feedback.

Table 1

Measurement of both lower limbs

Name	Variation	Group	Average length	SD
Left limb	No	10	832.128 mm	0.105
Right limb	No	10	832.298 mm	0.083
Left limb	Down 5 mm	10	837.189 mm	0.024
Left limb	Down 10 mm	10	842.597 mm	0.038

two lower limbs were 4.891 and 10.299 mm, respectively. In the aforementioned experiment, the measurement error of the mean difference between the two lower limbs, after discounting the movements of the affected limb, was within 0.3 mm (0.219 and 0.299mm respectively).

4.3. End-Effector Control

The motor of the end-effector implied the grinding scheme according to the instructions for grinding the model of cartilage and hipbone. As shown in Figure 13a and 13c, the end-effector file could fulfill normal ground. As shown in Figure 13b and 13d, it could stop and exit with an emergency shutdown when reaching a pressure value of 30 N.

5. CONCLUSION

This paper proposes a robotic system for THA surgery equipped with functionalities for high-accuracy positioning of the preoperatively planned target and grinding angle during surgery. In addition, we propose an accurate intraoperative measurement system based on optical probes, which

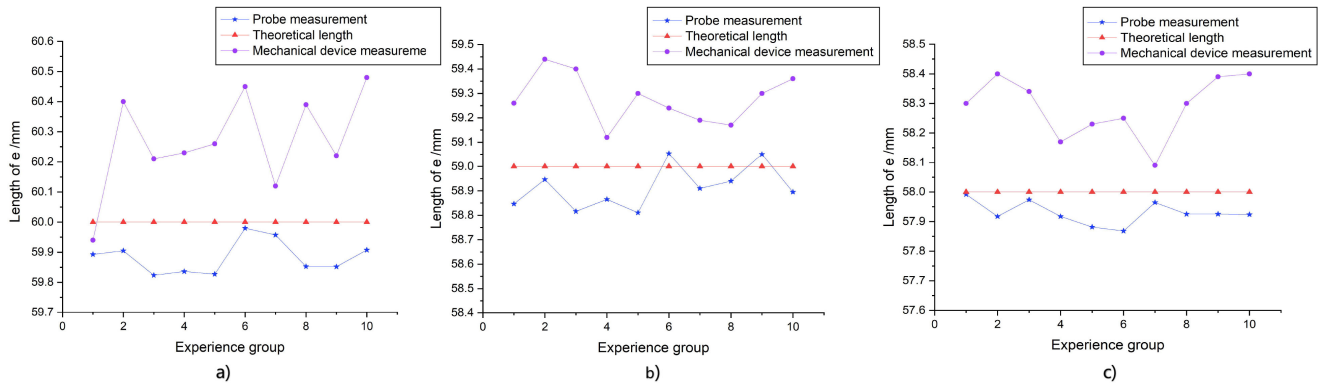


Figure 12: Comparison of distance e from highest point of femoral bulb prosthesis to osteotomy surface. a), b), and c) indicate red, blue, and white femoral heads, respectively, corresponding to different measured values e .

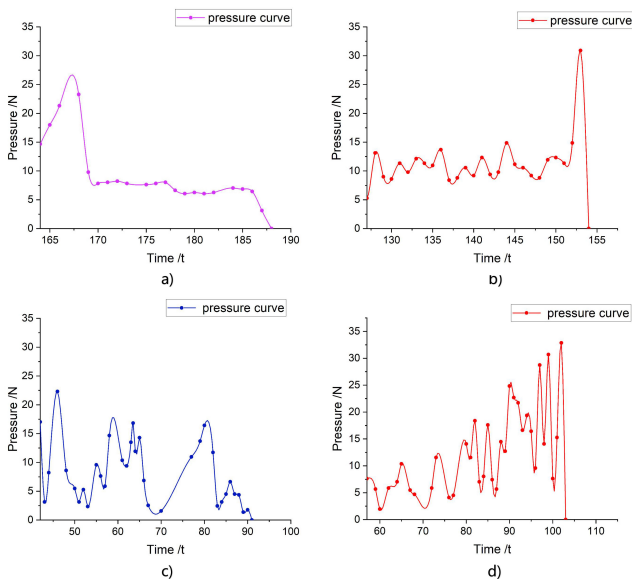


Figure 13: Grinding pressure change curve. a) normal pressure withdrawal during grinding of cartilage model; b) excessive pressure withdrawal during grinding of cartilage model; c) normal pressure withdrawal during grinding of bone model; d) excessive pressure withdrawal during grinding of bone model.

measures the femoral neck length and the difference between the two lower limbs in real-time during the operation. This can effectively assist surgeons in making surgical decisions and selecting appropriate prostheses to minimise preoperative errors. A limitation of this study is that the results are only achieved by simulated experiments. In the next step, we will apply the developed system to clinical trials for further verification.

References

- [1] Stephen Petis, James L Howard, Brent L Lanting, and Edward M Vasarhelyi. Surgical approach in primary total hip arthroplasty: anatomy, technique and clinical outcomes. *Canadian Journal of Surgery*, 58(2):128, 2015.
- [2] Huijuan Cao, Hanfeng Guan, Yuxiao Lai, Ling Qin, and Xinluan Wang. Review of various treatment options and potential therapies for osteonecrosis of the femoral head. *Journal of orthopaedic translation*, 4:57–70, 2016.
- [3] Andrew J Hall and Edward Dunstan. Day-case total hip arthroplasty: a safe and sustainable approach to improve satisfaction and productivity, and meet the needs of the orthopaedic population. *Orthopaedics and Trauma*, 36(1):14–21, 2022.
- [4] Vishal Kumar, Sandeep Patel, Vishnu Baburaj, Rajesh Kumar Rajnish, and Sameer Aggarwal. Does robotic-assisted surgery improve outcomes of total hip arthroplasty compared to manual technique? a systematic review and meta-analysis. *Postgraduate Medical Journal*, 2021.
- [5] Andrea Marcovigi, Dario Sandoni, Luigi Ciampalini, Piergiuseppe Perazzini, Francesco Zambianchi, William J Hozack, and Fabio Catani. Dislocation risk after robotic arm-assisted total hip arthroplasty: a comparison of anterior, lateral and posterolateral approaches. *HIP International*, page 11207000221094513, 2022.
- [6] Sebastien Parratte and Jean-Noel A Argenson. Validation and usefulness of a computer-assisted cup-positioning system in total hip arthroplasty: a prospective, randomized, controlled study. *JBJS*, 89(3):494–499, 2007.
- [7] George E Lewinnek, JL Lewis, RICHARD Tarr, CL Compere, and JR Zimmerman. Dislocations after total hip-replacement arthroplasties. *J Bone Joint Surg Am*, 60(2):217–220, 1978.
- [8] Thomas Kalteis, M Handel, T Herold, Lars Perlick, H Baethis, and Joachim Grifka. Greater accuracy in positioning of the acetabular cup by using an image-free navigation system. *International orthopaedics*, 29(5):272–276, 2005.
- [9] G Saxler, A Marx, D Vandeveldel, U Langlotz, M Tannast, M Wiese, U Michaelis, G Kemper, PA Grützner, R Steffen, et al. The accuracy of free-hand cup positioning-a ct based measurement of cup placement in 105 total hip arthroplasties. *International orthopaedics*, 28(4):198–201, 2004.
- [10] Karl-Heinz Widmer. A simplified method to determine acetabular cup anteversion from plain radiographs. *The Journal of arthroplasty*, 19(3):387–390, 2004.
- [11] Charles L DeChenne, Uma Jayaram, Tim Lovell, Nick Dong, and Mike Cusick. A novel acetabular alignment guide for thr using selective anatomic landmarks on the pelvis. *Journal of biomechanics*, 38(9):1902–1908, 2005.
- [12] Nathaniel J Stewart, James L Stewart, and Abra Brisbin. A comparison of component positioning between fluoroscopy-assisted and robotic-assisted total hip arthroplasty. *The Journal of Arthroplasty*, 2022.
- [13] Christian Plaass, Martin Clauss, Peter E Ochsner, and Thomas Ilchmann. Influence of leg length discrepancy on clinical results after

- total hip arthroplasty—a prospective clinical trial. *Hip international*, 21(4):441–449, 2011.
- [14] Isao Asayama, Samatchai Chamnongkich, Kathy J Simpson, Tracy L Kinsey, and Ormonde M Mahoney. Reconstructed hip joint position and abductor muscle strength after total hip arthroplasty. *The Journal of arthroplasty*, 20(4):414–420, 2005.
- [15] Kyoichi Ogawa, Tamon Kabata, Toru Maeda, Yoshitomo Kajino, and Hiroyuki Tsuchiya. Accurate leg length measurement in total hip arthroplasty: a comparison of computer navigation and a simple manual measurement device. *Clinics in Orthopedic Surgery*, 6(2):153–158, 2014.
- [16] Hiroaki Tagomori, Nobuhiro Kaku, Tomonori Tabata, and Hiroshi Tsumura. A new and simple intraoperative method for correction of leg-length discrepancy in total hip arthroplasty. *Journal of orthopaedics*, 16(5):405–408, 2019.
- [17] Runzhi Xia, Zanjing Zhai, Jingwei Zhang, Degang Yu, Liao Wang, Yuanqing Mao, Zhenan Zhu, Haishan Wu, Kerong Dai, Mengning Yan, et al. Verification and clinical translation of a newly designed “skywalker” robot for total knee arthroplasty: a prospective clinical study. *Journal of Orthopaedic Translation*, 29:143–151, 2021.
- [18] Zhonghua Xu and Yuan Zhang. What’s new in artificially intelligent joint surgery in china? the minutes of the 2021 ieee icra and literature review. *Arthroplasty*, 4(1):1–11, 2022.
- [19] Chelsea S Sicat, Daniel B Buchalter, Tyler A Luthringer, Ran Schwarzkopf, and Jonathan M Vigdorichik. Intraoperative technology use improves accuracy of functional safe zone targeting in total hip arthroplasty. *The Journal of Arthroplasty*, 2022.
- [20] Brian Davies, Matjaz Jakopc, Simon J Harris, F Rodriguez Y Baena, Adrian Barrett, Alexander Evangelidis, Paula Gomes, Johan Henckel, and Justin Cobb. Active-constraint robotics for surgery. *Proceedings of the IEEE*, 94(9):1696–1704, 2006.
- [21] Samik Banerjee, Jeffery J Cherian, Randa K Elmallah, Todd P Pierce, Julio J Jauregui, and Michael A Mont. Robot-assisted total hip arthroplasty. *Expert review of medical devices*, 13(1):47–56, 2016.
- [22] Zheng Li, Xin Chen, Xiaoquan Wang, Bo Zhang, Wei Wang, Yu Fan, Jun Yan, Xiaofeng Zhang, Yu Zhao, Yuan Lin, et al. Hurwa robotic-assisted total knee arthroplasty improves component positioning and alignment—a prospective randomized and multicenter study. *Journal of Orthopaedic Translation*, 33:31–40, 2022.
- [23] Fiachra E Rowan, Biju Benjamin, Jurek R Pietrak, and Fares S Haddad. Prevention of dislocation after total hip arthroplasty. *The Journal of Arthroplasty*, 33(5):1316–1324, 2018.
- [24] Nobuhiko Sugano. Computer-assisted orthopaedic surgery and robotic surgery in total hip arthroplasty. *Clinics in orthopedic surgery*, 5(1):1–9, 2013.
- [25] Arndt P Schulz, Klaus Seide, Christian Queitsch, Andrea Von Haugwitz, Jan Meiners, Benjamin Kienast, Mohamad Tarabolsi, Michael Kammal, and Christian Jürgens. Results of total hip replacement using the robodoc surgical assistant system: clinical outcome and evaluation of complications for 97 procedures. *The International Journal of Medical Robotics and Computer Assisted Surgery*, 3(4):301–306, 2007.
- [26] Padmanabhan Subramanian, Tom W Wainwright, Shayan Bahadori, and Robert G Middleton. A review of the evolution of robotic-assisted total hip arthroplasty. *Hip International*, 29(3):232–238, 2019.
- [27] Christopher J Hadley, Eric L Grossman, Michael A Mont, Hytham S Salem, Fabio Catani, and Andrea Marcovigi. Robotic-assisted versus manually implanted total hip arthroplasty: A clinical and radiographic comparison. *Surgical technology international*, 37, 2020.
- [28] Pascal Kouyoumdjian, Jad Mansour, Chahine Assi, Jacques Caton, Sebastien Lustig, and Remy Coulomb. Current concepts in robotic total hip arthroplasty. *SICOT-J*, 6, 2020.
- [29] Itay Perets, Brian H Mu, Michael A Mont, Gurion Rivkin, Leonid Kandel, and Benjamin G Domb. Current topics in robotic-assisted total hip arthroplasty: a review. *Hip International*, 30(2):118–124, 2020.
- [30] Olga Sorkine-Hornung and Michael Rabinovich. Least-squares rigid motion using svd. *Computing*, 1(1):1–5, 2017.
- [31] Nghia Ho. Finding optimal rotation and translation between corresponding 3d points. URL <http://nghiaho.com>, 2013.
- [32] Lingxiang Zheng, Han Wu, Lin Yang, Yonghua Lao, Qinyong Lin, and Rongqian Yang. A novel respiratory follow-up robotic system for thoracic-abdominal puncture. *IEEE Transactions on Industrial Electronics*, 68(3):2368–2378, 2020.

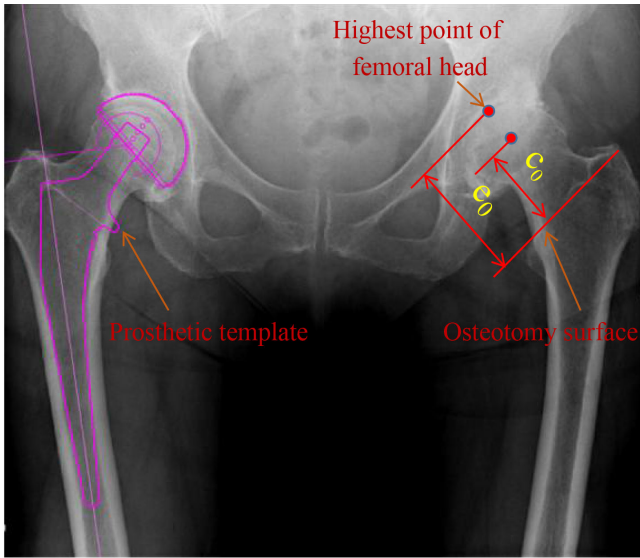


Figure 14: Preoperative planning of desired femoral neck length.

6. APPENDIX

6.1. Desired femoral neck length

As shown in Figure 14, the patient's right acetabulum was normal, but with defected in the left acetabulum development. According to the principle of symmetry, the position of the left osteotomy surface could be planned with reference to the right side before operation. If we measured the vertical distance e from the highest point of the femoral head to the osteotomy surface, we could then obtain the desired value c_0 of the preoperative femoral neck length from the formula $c_0 = e_0 - r$, where r was the rotation radius of the femoral head. Finally, according to the length of the femoral neck, the inner diameter of the femoral medullary cavity and the insertable depth of the femoral medullary cavity, the model of the prosthesis able to be fit into the medullary cavity could be obtained from the manual. Figure 14 showed the template of the acetabular prosthesis implanted on the left side.

6.2. Intraoperative Navigation Measurement

As shown in Figure 15, after the femoral stem prosthesis was installed, the length e from the highest point to the osteotomy surface was measured using a probe. Based on the desired value from preoperative measurement, a comparison between the selected femoral bulb and femoral neck prosthesis was performed. Thus, the final femoral bulb prosthesis could be accurately selected. We prepared three different depth models of red, blue, and white femoral head prostheses (Figure 16) and made reasonable adjustments to compensate for preoperative errors according to the femoral neck length measured in real time. Subsequently, the length of both lower limbs for the selected prosthesis was measured for further verification and feedback.

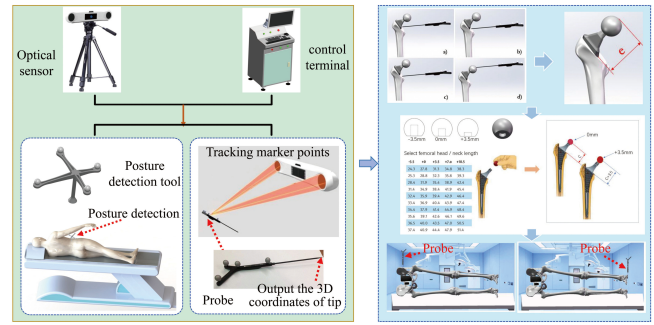


Figure 15: Intraoperative measurements and navigation based on optical positioning.

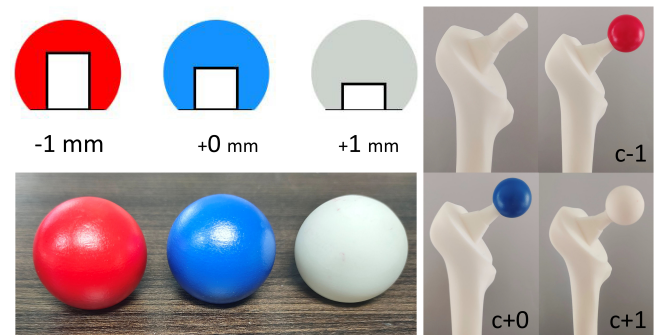


Figure 16: Selection of prosthetic specifications; c is actual length from rotation centre to osteotomy surface.

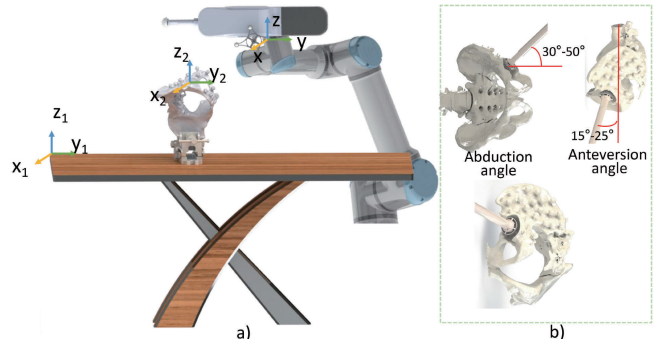


Figure 17: Simulation of calibration protocol for intraoperative localisation initialisation.

6.3. Real-time Measurement of Grinding Angle

The hip was fixed in the lateral recumbent position on the platform forceps, and calibration initialisation was performed on the end-effector parallel to the hip model (Figure 17a). The relative angles of the tools on the end-effector with attached marker balls were the abduction angle and forward tilt angle of the intraoperative reamer (Figure 17b). The placement of optical monitoring tools simulated intraoperative real-time observations of changes in hip position.